Journal of Theoretical and Applied Physics (2020) 14:251–259
https://doi.org/10.1007/s40094-020-00378-1

RESEARCH

Effect of thickness on characteristics of ZnSe thin film synthesized by vacuum thermal evaporation

Md. Abu Sayeed[1] · Hasan Khaled Rouf[1] · Kazi Md. Amjad Hussain[2]

Received: 6 December 2019 / Accepted: 22 May 2020 / Published online: 2 June 2020
© Islamic Azad University 2020

Abstract
Zinc selenide (ZnSe) thin films with various thicknesses were grown on ultrasonically clean glass substrates using vacuum evaporation of 99.99% pure ZnSe powder. Thickness dependence of the structural, optical and electrical properties was thoroughly investigated. X-ray diffraction (XRD) analyses revealed that (110) ZnSe plane is the dominant crystal plane for all the fabricated films. Both dislocation density and micro-strain go down with the increase in film thickness, indicating lower lattice defects and improvement in crystallinity at higher film thickness. Transmittance spectra show that all the films have almost linear upward tendency of transmittance in near-infrared region and small fluctuations in visible region for higher-thickness films. With the increase in film thickness, the optical bandgap increases and also an increasing tendency of dielectric constant was observed. Studies of electrical properties showed a sharp increase in carrier mobility and concentration with film thickness. As the film thickness increases from 30 to 90 nm, the carrier mobility goes up from 255 to 1250 cm^2/VS and the carrier concentration increases from 2.14×10^{18} to 9.37×10^{18} cm^{-3}. The electrical transport properties of the deposited thin films were explained in terms of scattering of the charge carrier.

Keywords ZnSe thin film · Vacuum thermal evaporation · X-ray diffraction · UV–Vis–NIR spectrophotometer · Hall effect measurement

Introduction

ZnSe, a direct bandgap II–VI group compound semiconductor, is a promising material for applications in optoelectronic devices, namely blue-green lasers, light-emitting diodes, optically controlled switches, dielectric mirrors and filters, solar cells, photoconductors and optically bi-stable devices [1–3]. Its properties such as direct wide bandgap of about 2.7 eV at room temperature, low electrical resistivity, high optical transmission, high luminescence and good photosensitivity make it advantageous for use as window (buffer) layer in chalcogenide-based thin-film solar cells [4–6]. As an alternative to mostly used toxic CdS, it is environmentally friendly and fits better in the solar spectrum [7]. For its high refractive index and low dispersion rate at infrared wavelengths, ZnSe has great potential to be used in infrared applications [8]. There are many reports on the growth of ZnSe thin films in various methods including thermal evaporation, electrochemical deposition, sputtering technique, metal–organic chemical vapor deposition (MOCVD) and chemical bath deposition [9–13].

Vacuum thermal evaporation technique is attractive because it uses a strong vacuum environment, and so is capable of producing very-high-purity thin films. Moreover, the deposition rate is high and damage to the substrate during deposition can be minimized. So far, many growth parameters have been optimized to achieve high-quality ZnSe thin films [14, 15]. However, the effects of thickness on the ZnSe film properties have not been much reported in the literature. In this work, ZnSe thin films of five different thicknesses ranging from 30 to 90 nm were deposited on glass substrates by using vacuum thermal evaporation technique. The effects due to the variation of film thicknesses on the

✉ Hasan Khaled Rouf
hasan.rouf@cu.ac.bd

Md. Abu Sayeed
sayeedrasel29@gmail.com

Kazi Md. Amjad Hussain
kazi326@yahoo.com

[1] Department of Electrical and Electronic Engineering, University of Chittagong, Chittagong 4331, Bangladesh

[2] Experimental Physics Division, Atomic Energy Center, Dhaka 1000, Bangladesh

structural, optical and electrical properties of ZnSe thin films were investigated. Phase identification and the crystalline structures of the samples were analyzed by an X-ray diffractometer. Optical properties of the deposited films were investigated by a dual-beam UV–Vis–NIR spectrophotometer. Electrical resistivity, conductivity and electron mobility of the grown thin films were measured by using the dc two-point probe method and the Hall effect measurement.

Experimental details

Zinc selenide thin films were fabricated using vacuum evaporation of 99.99% pure ZnSe powder on a soda lime glass substrate which was cleaned ultrasonically in acetone solution followed by rinsing with deionized water. After rinsing, glass substrate was kept inside a vacuum desiccator which was filled with moisture-absorbing silica gel for 20 h to dry. Coarse ZnSe was crushed into fine powder and put into molybdenum (Mo) boat used as evaporation source inside the vacuum chamber of the evaporator (NIRVAT: EU-300). The cleaned substrate was clamped directly on top of the evaporation source with tin mask to control deposition area.

The whole fabrication process was carried out at a vacuum pressure of approximately 10^{-4} Pa, and the deposition rate was controlled by manual adjustment of Variac (VACTECH: APMG-053). The substrate temperature was kept at 290 °C, while the deposition rate and thickness of the film were monitored by quartz crystal oscillator. The deposition rate was around 0.3 nm/sec, and the thickness varied from 30 to 90 nm. Deposited ZnSe thin films were then annealed at 300 °C for 60 min to ensure against contamination due to oxidation of the films.

Phase identification and the crystalline structures of the samples were analyzed by an X-ray diffractometer (Philips X'Pert PW-3040) using Bragg–Brentano diffraction geometry. The diffractometer was operating at 40 kV, 35 mA, and the measurements were carried out at room temperature. The optical properties of ZnSe thin films were investigated by a dual-beam UV–Vis–NIR spectrophotometer (Shimadzu UV-3600, MPC-3100), and the electrical resistivity, conductivity and electron mobility of the grown thin films were measured by using the dc two-point probe method and the Hall effect measurement.

Results and discussion

Structural characterization

Structural characterization of the films produced was examined using XRD analyses. Figure 1 shows X-ray diffraction patterns of ZnSe thin films at different thicknesses grown on glass substrates. The XRD patterns show that the film of 30 nm thickness exhibited four diffraction peaks of (100), (110), (111) and (200) planes of ZnSe. For 40-nm ZnSe thin film, a prominent intensity was observed for the (100) and (110) planes. However, as the film thickness increases, the XRD intensity peak of the (110) plane increases drastically, whereas those of the other planes remain almost the same. Thus, the film of 90 nm thickness has the only diffraction peak of (110) plane. Therefore, the (110) ZnSe plane is the dominant crystal plane for all the fabricated films.

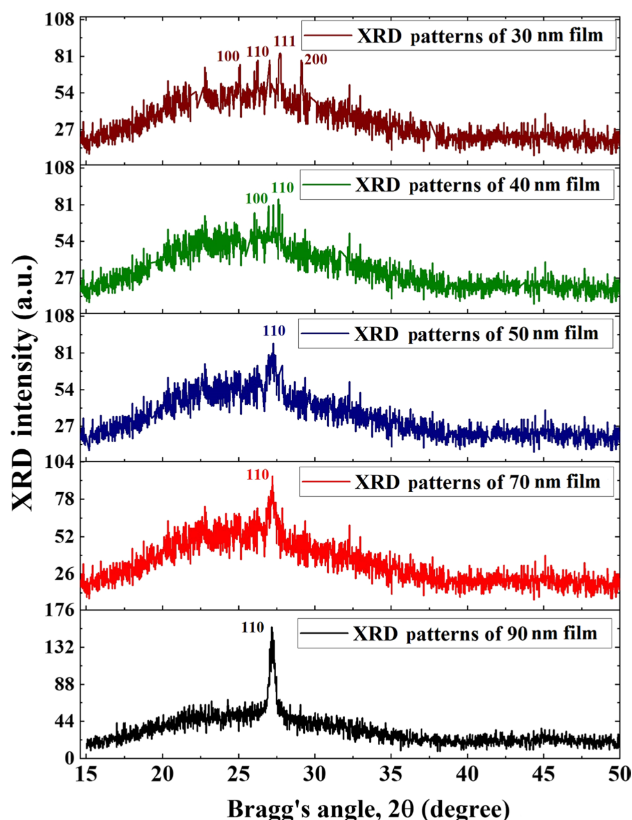

Fig. 1 XRD patterns of ZnSe films produced by thermal evaporation at 290 °C on glass substrate

Thin film with higher thickness possesses more stacked or immobile electrons in lattice, and X-ray photons only interact with stacked electrons and reflected back to the detector placed in the diffractometer. Using the XRD patterns, interplanar spacing or d-spacing (Angstrom) was calculated for all the five film thicknesses and is shown in Table 1. From the XRD data, lattice constant (a) of the prepared ZnSe films was also calculated by using the following equation [16]:

$$d = \frac{a}{\sqrt{\left(h^2 + k^2 + l^2\right)}} \tag{1}$$

where h, k, l are the miller indices of the plane and d is the interplanar spacing. Figure 2 graphically shows the

Table 1 Interplanar spacing (*d*-spacing) for different film thicknesses

ZnSe film thickness	Planes	*d*-spacing (Å)
30 nm	100	5.6851
	110	4.0267
	111	3.2925
	200	2.8601
40 nm	100	5.6614
	110	4.0109
50 nm	110	3.9936
70 nm	110	3.9542
90 nm	110	5.5413

calculated lattice constants of five ZnSe thin films, and for convenience, a unit cell structure of the fabricated ZnSe thin film is presented in Fig. 3, which shows a face-centered cubic (fcc) structure. Due to surface reconstruction near the crystal surface, lattice constant deviates from its average value which is crucial in nanocrystal surface because of its large core ratio.

From the XRD measurements, mean crystallite sizes or grain sizes (S_c) of the films were evaluated using the Debye–Scherrer equation [17]:

$$S_c = \frac{K \times \lambda}{\beta \times \cos\theta} \quad (2)$$

Here, K is dimensionless shape factor which is 0.94 in this case, λ is the wavelength of X-ray photon which is 1.54 Å, β is full width at half maximum (FWHM) and θ is the Bragg's angle in diffractometer. Full width at half maximum (β) and Bragg's angle (θ) for films having different thicknesses are shown in Table 2, and the corresponding mean crystallite sizes are shown in Fig. 4. As the ZnSe film thickness increases, the grain size also increases from 19.4 to 33.8 nm. Higher compressive stress exists in the films having higher thickness, and such films have lower mean effective tensile elastic stress during grain growth. This results in increase in grain size. Micro-strain (M_S) affects many properties such as film strength, cracking and hardness and helps to check the critical limit of elasticity. This parameter was calculated by using the following equation [18]:

$$M_S = \frac{\beta \times \cos\theta}{4} \quad (3)$$

A graphical representation of micro-strain is shown in Fig. 5 from which we can observe, as the film thickness increases, micro-strain decreases throughout the lattice, which implies that lower-thickness ZnSe films have relatively higher lattice mismatches. Now on the basis of Williamson and Smallman method, dislocation density (ρ) was calculated using [19, 20]:

$$\rho = \frac{15 \times M_s}{a \times S_c} \quad (4)$$

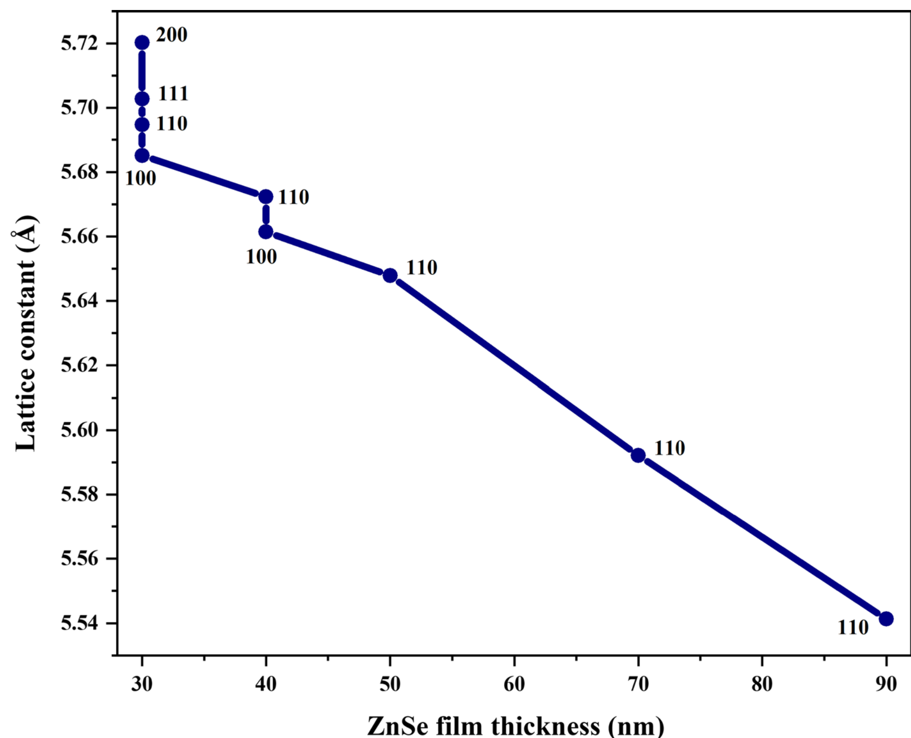

Fig. 2 Variation of lattice constant of films of different thicknesses obtained for different planes

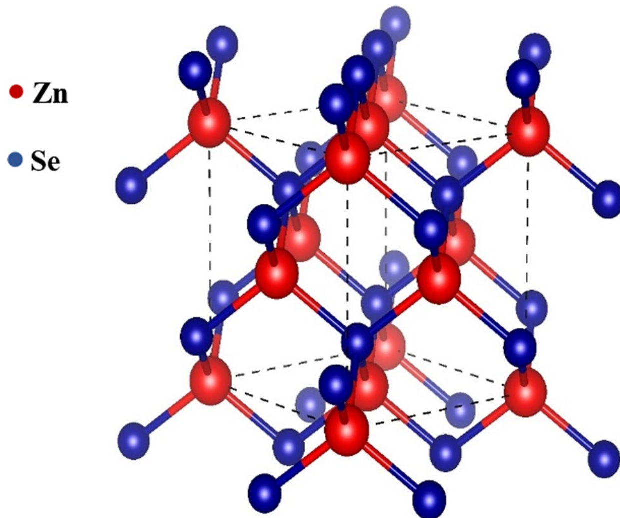

Fig. 3 Unit cell structure of the fabricated ZnSe thin film

Table 2 Bragg's angle and FWHM for films of different thicknesses

ZnSe film thickness	Bragg's angle (θ)	FWHM (β)
30 nm	13.8°	0.0254 rad
40 nm	13.7°	0.0187 rad
50 nm	13.80°	0.0152 rad
70 nm	13.74°	0.0124 rad
90 nm	13.58°	0.0081 rad

Here, M_S is the micro-strain, a is the lattice constant and S_c is the crystallite size. Since crystallite size increases with film thickness (Fig. 4), the above equation dictates that both dislocation density and micro-strain go down with the increase in film thickness. A graphical representation of this is shown in Fig. 6. The decrease in the dislocation density and strain with increasing film thickness indicates very few lattice defects and the formation of films with good crystalline qualities. Thus, the 90-nm film has less defects in its lattice structure than the 50-nm film.

Optical characterization

Figure 7 shows the transmittance curves of ZnSe thin films with different thicknesses. All the films have almost linear upward tendency of transmittance in near-infrared region and small fluctuation in visible region for higher-thickness films. As the film thickness decreases, corresponding transmittance increases up to a maximum of 93% for 30-nm film which gets minimum for 90-nm film at certain wavelengths. Films having thicknesses of 90 nm and 70 nm have small variations in near-infrared region. Films with higher thicknesses have larger XRD intensity, i.e., greater number of stacked electrons than free electrons. Most of the incoming photons in spectrophotometer are reflected by these stacked electrons in 90-nm-thick film, and consequently, it has lowest transmittance. Conversely, the 30-nm film has the highest transmittance.

The optical absorption coefficient (α) can be calculated in the strong absorption region using the Beer–Lambert relationship [21]:

$$\alpha = \frac{1}{t} \ln \frac{1}{T} \tag{5}$$

where t and T are the film thickness and transmittance, respectively. In the high absorption region, the optical

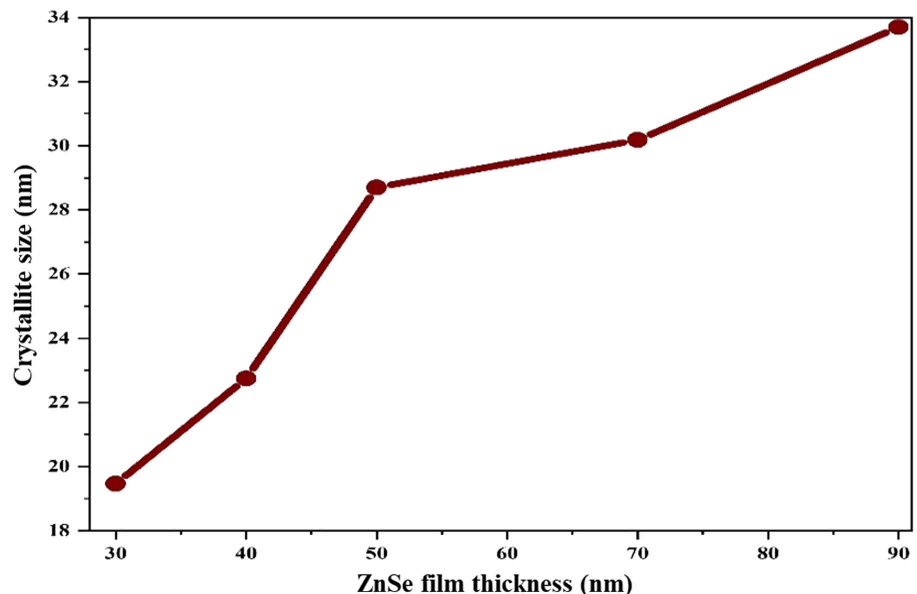

Fig. 4 Variation of crystallite size of ZnSe films produced on glass substrate with film thickness

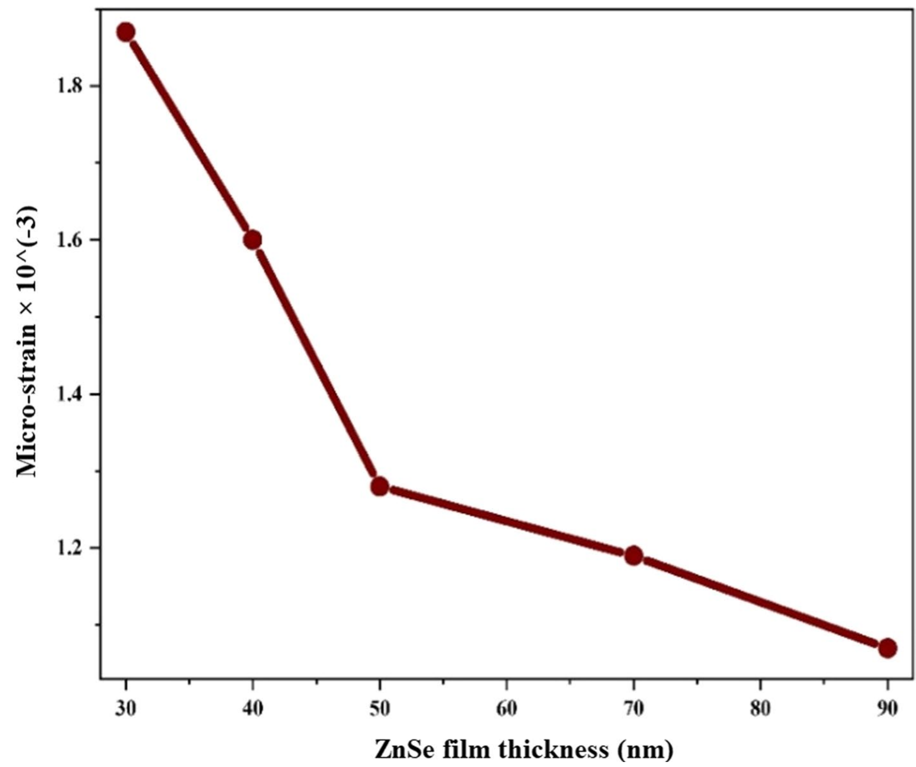

Fig. 5 Variation of micro-strain of the prepared ZnSe thin films with thickness

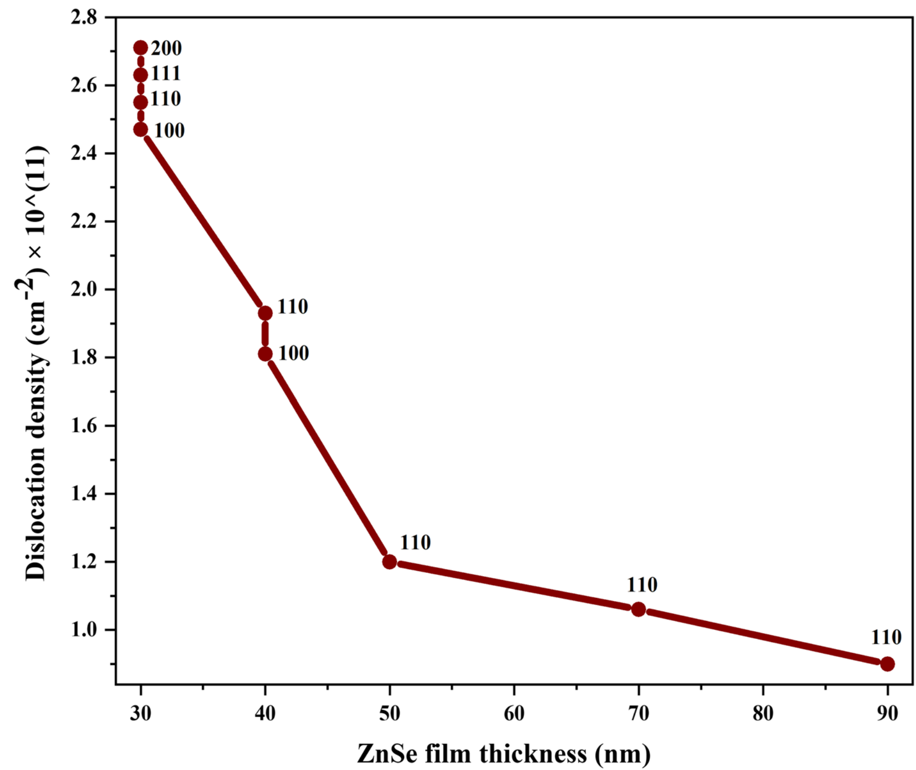

Fig. 6 Variation of dislocation density with film thickness obtained for different planes

bandgap (E_g) can be estimated by assuming a direct transition between the valence and conduction band using the Tauc's model [22, 23]:

$$(\alpha h\nu)^2 = B(h\nu - E_g) \quad (6)$$

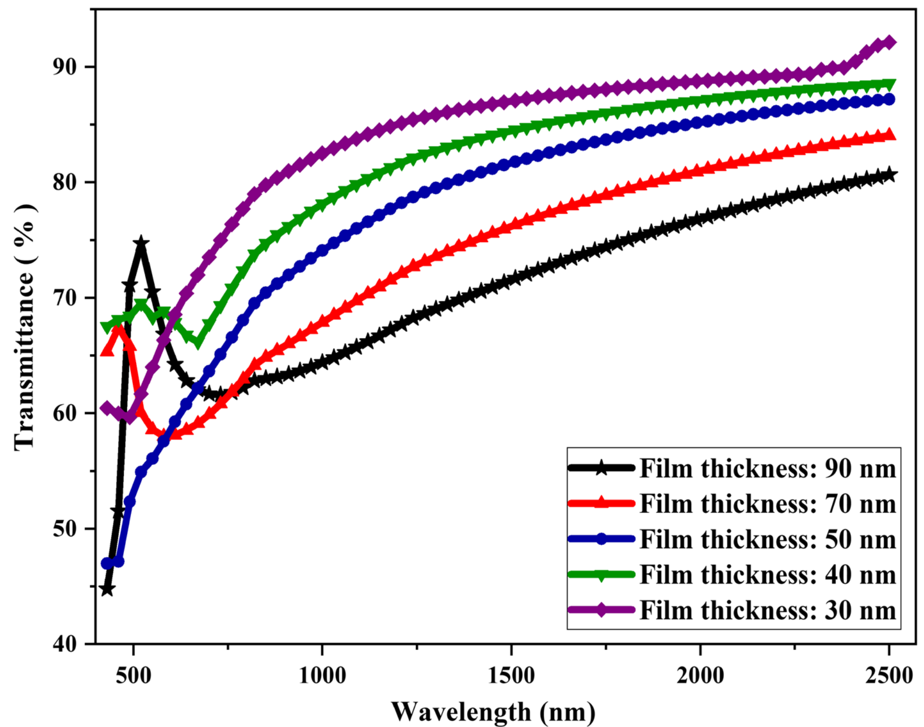

Fig. 7 Optical transmittance of ZnSe thin films for varying thicknesses

In Eq. (6), E_g is the optical bandgap, $h\nu$ is the energy of the incident photon and B is an energy-independent constant. Therefore, a plot of $(\alpha h\nu)^2$ versus photon energy $(h\nu)$ produces a straight line that cut the photon energy axis at the optical bandgap value. Figure 8 shows the plot of $(\alpha h\nu)^2$ versus $h\nu$ for the prepared samples having five different thicknesses. The values of energy bandgap achieved from these plots show that as the ZnSe film thickness increases from 30 to 90 nm, the optical bandgap increases from 2.49 to 2.64 eV. As films with higher thicknesses have greater number of stacked electrons than free electrons, they have lower electrons in conduction band than valence band to conduct electricity. This shortage of electrons in conduction band makes the optical bandgap wider. On the other hand, films with lower thicknesses have relatively narrow bandgap and have potential applications in lasers, optical switches, dielectric mirrors, solar cells and high electron mobility transistors.

Refractive index (n) was obtained from reflectance (R) (*i.e.,* inverse of transmittance) and extinction coefficient (k) using the equation [24]:

$$n = \frac{1+R}{1-R} + \sqrt{\frac{4R + (1-R)^2 K^2}{(1-R)^2}} \tag{7}$$

Extinction coefficient and absorption coefficient were calculated by using the following equations [24]:

$$K = \frac{\alpha\lambda}{4\pi} \tag{8}$$

$$\alpha = \frac{1}{t}\ln\frac{(n-1)(n-n_s)}{(n+1)(n-n_s)}\left[\frac{\sqrt{\frac{T_M}{T_m}}+1}{\sqrt{\frac{T_M}{T_m}}-1}\right] \tag{9}$$

Here, t is the film thickness, n_s is the refractive index of glass substrate (1.52), and T_M and T_m are maximum and minimum transmittances measured at the same wavelength. Refractive index profile based on experimental data is shown in Table 3. Refractive index was observed to increase as the film thickness increases. Absolute dielectric constant can be calculated using the following equation:

$$dk = \sqrt{\left(n^2 - k^2\right)^2 + (2nk)^2} \tag{10}$$

where $(n^2 - k^2)$ and $2nk$ are, respectively, the real and imaginary parts of the dielectric constant. Table 3 shows the values of absolute dielectric constants for different thicknesses of ZnSe films. An increasing tendency of absolute dielectric constant with film thickness is observed.

Electrical characterization

Studies of electrical properties of the grown ZnSe thin films and the effects of film thickness on various electrical parameters were performed by using the dc two-point probe

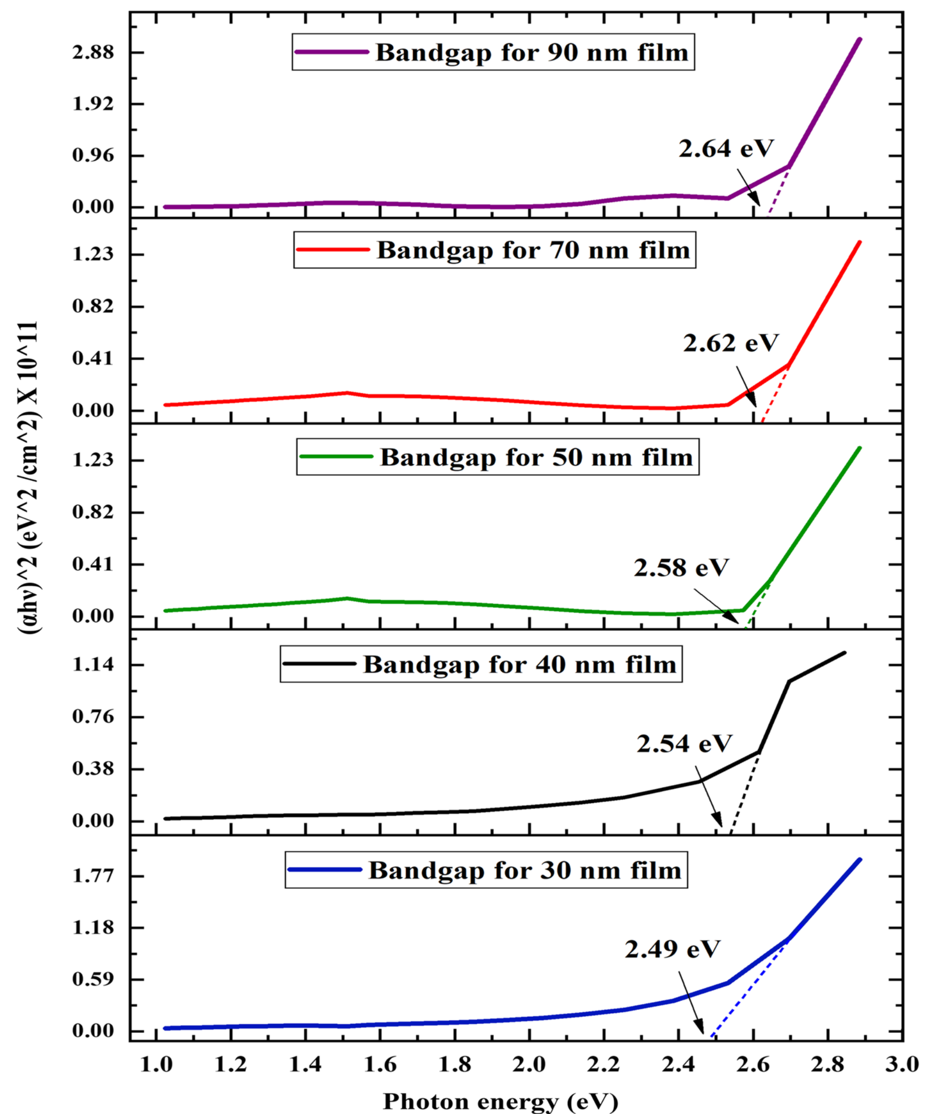

Fig. 8 Values of the optical bandgap for ZnSe films with different thicknesses by extrapolating the linear portions of the curves of $(\alpha h\nu)^2$ versus photon energy ($h\nu$)

Table 3 Values of refractive index and absolute dielectric constant for various film thicknesses

ZnSe film thickness	Refractive index	Absolute dielectric constant
30 nm	2.401	7.11
40 nm	2.470	7.33
50 nm	2.497	7.88
70 nm	2.556	8.94
90 nm	2.604	9.26

method and the Hall effect measurement. Figure 9 shows the current density–voltage characteristics of ZnSe thin films having five different thicknesses. The current density–voltage (*J*–*V*) curves were found to be almost symmetric and linear up to the operating range of external voltage. The ohmic conduction is dominant in the whole voltage range, and the number of free carriers is more than that of the injected ones in this region. Thin films having lower thicknesses have relatively higher current density since they have narrower optical bandgap compared to the films with higher thicknesses.

By using Hall effect measurements in van der Pauw configuration, electrical properties such as carrier mobility, average Hall coefficient, resistivity and carrier concentration were estimated for different film thicknesses and are presented in Table 4. It is seen that as the film thickness increases from 30 to 90 nm, the resistivity increases from 51.8×10^5 to 93.46×10^5 Ω cm and carrier concentration increases from 2.14×10^{18} to 9.37×10^{18} cm^{-3}. We also observe that the carrier mobility and the average Hall coefficient increase with the thickness of the films. For example, the carrier mobility goes up from 255 cm^2/VS for 30-nm film to 1250 cm^2/VS for 90-nm film. The average

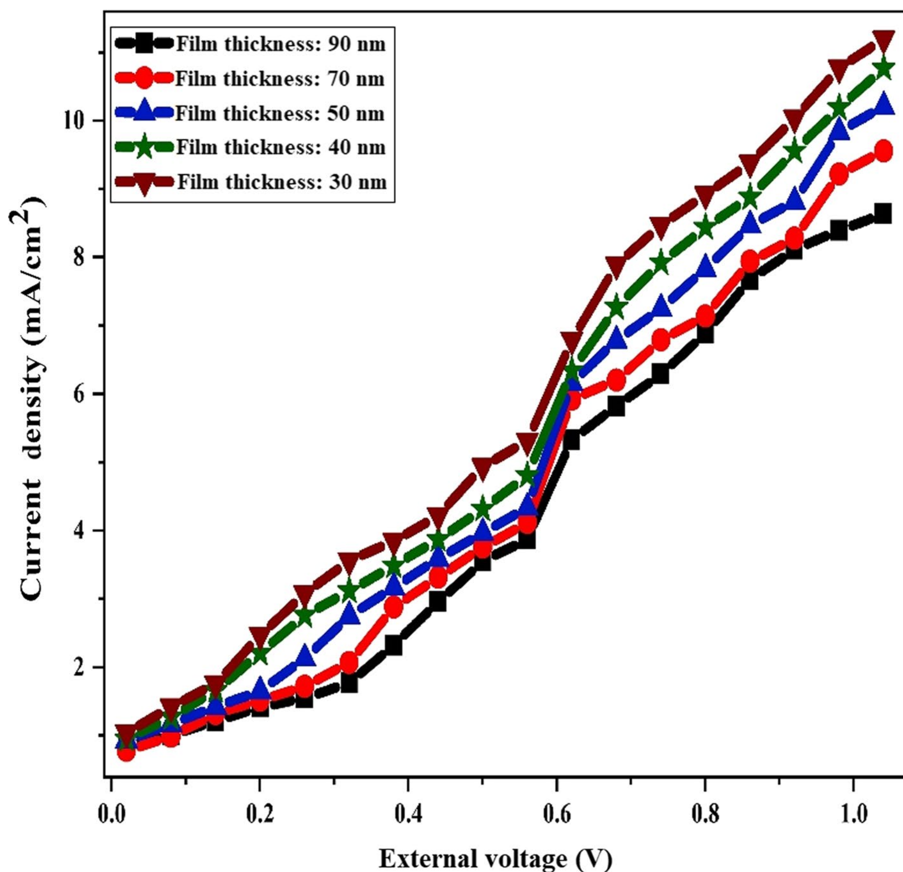

Fig. 9 Current density versus voltage (*J*–*V*) curves of the produced ZnSe thin films

Table 4 Electrical properties of ZnSe thin films for various film thicknesses

ZnSe film thickness (nm)	Mobility (cm^2/VS)	Hall coefficient (cm^3/C)	Resistivity (Ωcm)	Carrier concentration (cm^{-3})
30	2.55×10^2	1.35×10^2	51.8×10^5	2.14×10^{18}
40	4.15×10^2	2.18×10^2	56.5×10^5	3.07×10^{18}
50	7.26×10^2	3.42×10^2	68.5×10^5	5.45×10^{18}
70	10.44×10^2	4.49×10^2	80×10^5	7.62×10^{18}
90	12.50×10^2	5.5×10^2	93.46×10^5	9.37×10^{18}

Hall coefficient increases from 135 to 550 cm^3/C when the film thickness increases from 30 to 90 nm.

The electrical transport properties of the deposited thin films can be explained in terms of scattering of the charge carrier. For semiconducting thin films deposited on nonconducting glass substrates, two types of charge carrier scattering can occur, namely interfacial scattering between thin film and substrate surface and grain boundary scattering. We discussed earlier that thicker films are more crystalline and have larger grain size. When the thickness is lower, grains are smaller and conduction is influenced by interfacial scattering. As the thickness increases, the crystallinity of the film is improved, which results in decreasing the role of grain boundary scattering. The growth of thin films in this manner leads to a possibility of decreasing carrier traps across the grain boundaries with increasing thickness. The mobility of the charge carriers is directly related to this phenomenon. Thus, when the thickness increases, the crystallinity is improved and the grain size increases; the reduced grain boundary scattering leads to increased electrical resistivity and improved carrier mobility.

Conclusion

ZnSe thin films with different thicknesses were successfully grown on glass substrates using vacuum thermal evaporation technique. From the XRD data of the prepared films, we see

(110) ZnSe plane is the dominant crystal plane in the growth condition. As the ZnSe film thickness increases, the grain size also increases, while the dislocation density decreases. The decrease in the dislocation density and micro-strain indicates very few lattice defects and the formation of films having good crystalline qualities. Transmittance spectra show that all the films have almost linear upward tendency of transmittance in near-infrared region and small fluctuations in visible region for higher-thickness films. Optical bandgap was calculated by using the absorption coefficient which was determined from the transmittance spectra and was found to increase with the film thickness. Also, an increasing tendency of dielectric constant with increased film thickness was observed. Studies of electrical properties reveal a sharp increase in carrier mobility and concentration with film thickness contributing to the increase in resistivity. Interpretations of electrical transport properties as a function of film thickness were provided.

References

1. Ullrich, B.: Comparison of the photocurrent of ZnSe/InSe/Si and ZnSe/Si heterojunctions. Mater. Sci. Eng., B **56**(1), 69–71 (1998)
2. Alfano, R.R., Wang, Q.Z., Jimbo, T., Ho, P.P., Bhargava, R.N., Fitzpatrick, B.J.: Induced spectral broadening about a second harmonic generated by an intense primary ultrashort laser pulse in ZnSe crystals. Phys. Rev. A **35**(1), 459 (1987)
3. Son, D., Jung, D.R., Kim, J., Moon, T., Kim, C., Park, B.: Synthesis and photoluminescence of Mn-doped zinc sulfide nanoparticles. Appl. Phys. Lett. **90**(10), 101910 (2007)
4. Khan, T.M., Zakria, M., Ahmad, M., Shakoor, R.I.: Optoelectronic study and annealing stability of room temperature pulsed laser ablated ZnSe polycrystalline thin films. J. Lumin. **147**, 97–106 (2014)
5. Simpson, J., Wang, S.Y., Stewart, H., Wallace, J., Adams, S.J.A., Hauksson, I., Prior, K.A., Cavenett, B.C.: Electrical and optical characterization of p-type ZnSe for diode laser structures. J. Electron. Mater. **22**(5), 431–435 (1993)
6. Khan, T.M., Mehmood, M.F., Mahmood, A., Shah, A., Raza, Q., Iqbal, A., Aziz, U.: Synthesis of thermally evaporated ZnSe thin film at room temperature. Thin Solid Films **519**(18), 5971–5977 (2011)
7. Chu, T.L., Chu, S.S., Chen, G., Britt, J., Ferekides, C., Wu, C.Q.: Zinc selenide films and heterojunctions. J. Appl. Phys. **71**(8), 3865–3869 (1992)
8. Khan, T.M., BiBi, T.: Compatibility and optoelectronic of ZnSe nano crystalline thin film. Chin. Phys. B **21**(9), 097303 (2012)
9. Kale, R.B., Lokhande, C.D., Mane, R.S., Han, S.H.: Use of modified chemical route for ZnSe nanocrystalline thin films growth: study on surface morphology and physical properties. Appl. Surf. Sci. **252**(16), 5768–5775 (2006)
10. Patidar, D., Rathore, K.S., Saxena, N.S., Sharma, K., Sharma, T.P.: Determination of optical and electrical properties of ZnSe thin films. J. Mod. Opt. **55**(18), 3041–3047 (2008)
11. Yoo, J.B., Fahrenbruch, A.L., Bube, R.H.: Effect of a thin intermediate zinc selenide layer on the properties of CuInSe2 solar cells. Solar Cells. **31**(2), 171–180 (1991)
12. Banerjee, S., Pal, R., Maity, A.B., Chaudhuri, S., Pal, A.K.: Nanocrystalline ZnSe films prepared by high pressure magnetron sputtering. Nanostruct. Mater. **8**(3), 301–312 (1997)
13. Pal, R., Maiti, B., Chaudhuri, S., Pal, A.K.: ZnSe films: preparation and properties. Vacuum **46**(11), 1255–1260 (1995)
14. Vanzetti, L., Bonanni, A., Bratina, G., Sorba, L., Franciosi, A., Lomascolo, M., Greco, D., Cingolani, R.: Influence of growth parameters on the properties of ZnSe-GaAs (001) heterostructures. J. Cryst. Growth **150**, 765–769 (1995)
15. Mitsuhashi, H., Mitsuishi, I., Mizuta, M., Kukimoto, H.: Coherent growth of ZnSe on GaAs by MOCVD. Jpn. J. Appl. Phys. **24**(8A), L578 (1985)
16. Khan, T.M.: Into the nature of Pd-dopant induced local phonon modes and associated disorders in ZnO; based on spatial correlation model. Mater. Chem. Phys. **153**, 248–255 (2015)
17. Khan, T.M., Bibi, T., Hussain, B.: Synthesis and optical study of heat-treated ZnO nanopowder for optoelectronic applications. Bull. Mater. Sci. **38**(7), 1851–1858 (2015)
18. Khan, T.M., Zakria, M., Shakoor, R.I., Raffi, M., Ahmad, M.: Mechanisms of composite-hydroxide-mediated approach for the synthesis of functional ZnO nanostructures and morphological dependent optical emissions. Adv. Mater. Lett **6**, 592–599 (2015)
19. Khan, T.M., Iqbal, A., Zakria, M.: Study of excitonic UV emission stability, green luminescence and bandgap tune-ability in wurtzite $(ZnO)_{1-x}(Cr_2O_3)_x$ composite. Vacuum **105**, 1–6 (2014)
20. Khan, T.M., Irfan, M.: Studies on the complex behavior of optical phonon modes in wurtzite $(ZnO)_{1-x}(Cr_2O_3)_x$. Appl. Phys. A **117**(3), 1275–1282 (2014)
21. Gümüs, C., Ozkendir, O., Kavak, H., Ufuktepe, Y.: Structural and optical properties of zinc oxide thin films prepared by spray pyrolysis method. Journal of Optoelectronics and Advanced Materials. **8**(1), 299–303 (2006)
22. Iqbal, A., Mahmood, A., Khan, T.M., Ahmed, E.: Structural and optical properties of Cr doped ZnO crystalline thin films deposited by reactive electron beam evaporation technique. Progress Nat Sci Mater Int **23**(1), 64–69 (2013)
23. Tauc, J., Grigorovici, R., Vancu, A.: Optical properties and electronic structure of amorphous germanium. Physica Status Solidi (b). **15**(2), 627–637 (1966)
24. Khan, T.M.: A comparative study of physical properties of pure and In-doped nanostructured ZnO polycrystalline thin film for optoelectronic applications. J. Mater. Sci. Mater. Electron. **25**(4), 1673–1680 (2014)

Publisher's Note Springer Nature remains neutral with regard to jurisdictional claims in published maps and institutional affiliations.